

## Strathprints Institutional Repository

Assi, Gustavo and Srinil, Narakorn and Freire, Cesar and Korkischko, Ivan (2014) *Experimental investigation of the flow-induced vibration of a curved cylinder in convex and concave configurations*. Journal of Fluids and Structures, 44. pp. 52-66. ISSN 0889-9746

Strathprints is designed to allow users to access the research output of the University of Strathclyde. Copyright © and Moral Rights for the papers on this site are retained by the individual authors and/or other copyright owners. You may not engage in further distribution of the material for any profitmaking activities or any commercial gain. You may freely distribute both the url (<http://strathprints.strath.ac.uk/>) and the content of this paper for research or study, educational, or not-for-profit purposes without prior permission or charge.

Any correspondence concerning this service should be sent to Strathprints administrator: <mailto:strathprints@strath.ac.uk>

# Experimental investigation of the flow-induced vibration of a curved cylinder in convex and concave configurations

Gustavo R. S. Assi<sup>a,\*</sup>, Narakorn Srinil<sup>b</sup>, Cesar M. Freire<sup>c</sup>, Ivan Korkischko<sup>c,\*\*</sup>

<sup>a</sup>*Department of Naval Architecture and Ocean Engineering, University of São Paulo, São Paulo, Brazil*

<sup>b</sup>*Department of Naval Architecture and Marine Engineering, University of Strathclyde, Glasgow, UK*

<sup>c</sup>*Department of Mechanical Engineering, University of São Paulo, São Paulo, Brazil*

---

## Abstract

Experiments have been conducted to investigate the two-degree-of-freedom vortex-induced vibration (VIV) response of a rigid section of a curved circular cylinder with low mass-damping ratio. Two curved configurations, a concave and a convex, were tested regarding the direction of the flow, in addition to a straight cylinder that served as reference. Amplitude and frequency responses are presented versus reduced velocity for a Reynolds number range between 750 and 15,000. Results for the curved cylinders with concave and convex configurations revealed significantly lower vibration amplitudes when compared to the typical VIV response of a straight cylinder. However, the concave cylinder showed relatively higher amplitudes than the convex cylinder which were sustained beyond the typical synchronisation region. We believe this distinct behaviour between the convex and the concave configurations is related to the wake interference taking place in the lower half of the curvature due to perturbations generated in the horizontal section when it is positioned upstream. Particle-image velocimetry (PIV) measurements of the separated flow along the cylinder highlight the effect of curvature on vortex formation and excitation revealing a complex fluid-structure interaction mechanism.

---

\*Corresponding author: g.assi@usp.br. Address: PNV Dept. Eng. Naval e Oceânica, Escola Politécnica da Universidade de São Paulo, Av. Prof Mello Moraes 2231, 05508-030, São Paulo - SP, Brazil. [www.ndf.poli.usp.br](http://www.ndf.poli.usp.br).

\*\*Now at the Institute of Aerodynamics and Flow Technology, German Aerospace Center (DLR), Göttingen, Germany.

*Keywords:*

Vortex-induced vibration, Cross-flow and in-line motion, Curved cylinder,  
Particle image velocimetry

---

## Nomenclature

$D$  Cylinder external diameter  
 $h$  Cylinder vertical length below the water line  
 $m^*$  Mass ratio  
 $\zeta$  Structural damping ratio  
 $f_0$  Natural frequency in air  
 $U$  Flow speed  
 $U/Df_0$  Reduced velocity  
 $\hat{x}$  Streamwise harmonic amplitude of vibration  
 $\hat{y}$  Cross-flow harmonic amplitude of vibration  
 $f_x$  Streamwise oscillation frequency  
 $f_y$  Cross-flow oscillation frequency  
Re Reynolds number

## 1. Introduction

Ongoing deep-sea exploration, installation and production of hydrocarbon energy need the development of new viable technologies. One of these is the requirement of a robust and reliable analysis tool for the prediction of vortex-induced vibration (VIV) of marine structures exposed to ocean currents. Because VIV can cause high cyclic-loading fatigue damage of structures, it is now widely accepted to be a crucial factor that should be taken into account in the preliminary analysis and design. However, many insightful VIV aspects are still unknown and far from fully understood; these render the structural design quite conservative with the use of a large factor of safety. For offshore structures with initial curvatures and high flexibility such as catenary risers, mooring cables and free-spanning pipelines, the theoretical, numerical or experimental VIV research is still very lacking.

Risers are very long pipes used to carry oil from the sea bed to offshore platforms floating on the water surface. Under the effect of sea currents, these flexible structures are especially susceptible to flow-induced vibrations, particularly since they have a relatively low mass compared to the mass of the displaced fluid. Generally, an offshore floating platform accommodates several riser pipes together with many other cylindrical structures. The

20 interaction of these flexible structures can produce an even more complex  
21 problem, resulting in vibrations with rather unexpectedly higher amplitudes  
22 (Assi et al., 2010). Flow interference from the platform hull, the soil on  
23 sea bed and the pipe itself can also increase the complexity of the flow,  
24 generating complex responses.

25 The riser may respond with different amplitudes and frequencies de-  
26 pending on the flow excitation and structural stiffness along the length of  
27 the pipe. Consequently, several modes of vibration with varying curvature  
28 appear along the span resulting in a very rich fluid-structure interaction  
29 mechanism (Srinil, 2010). In addition to that, flexible risers can be laid  
30 out in a catenary configuration which results in high curvature close to the  
31 region where it touches the bottom of the ocean, called the touchdown point.

32 In an attempt to understand and model the fluid-dynamic behaviour  
33 around curved sections of risers we have performed experiments with a  
34 curved, rigid circular cylinder in a water channel. This idealised experi-  
35 ment is far from reproducing the real conditions encountered in the ocean;  
36 nevertheless it should throw some light on understanding how the vortex  
37 shedding mechanism is affected by the curvature of the pipe. In addition to  
38 the phenomenological aspects, the present work may also serve as reference  
39 for validation and benchmarking of numerical simulations of fluid-structure  
40 interaction.

41 An investigation into the vortex shedding patterns and the fundamental  
42 wake topology of the flow past a stationary curved circular cylinder has been  
43 carried out by Miliou et al. (2007) based on computational fluid dynamics  
44 studies. As a result of pipe initial curvatures, flow visualizations highlight  
45 different kinds of wake characteristics depending on the pipe (convex or  
46 concave) configuration and its orientation with respect to (aligned with or  
47 normal to) the incoming flow. When the flow is uniform and normal to  
48 the curvature plane, the cross-flow wake dynamics of curved pipes behave  
49 qualitatively similar to those of straight pipes. This is in contrast to the  
50 case of flow being aligned with the curvature plane where wake dynamics  
51 change dramatically. However, these scenarios are pertinent to a particular  
52 stationary cylinder case in a very low-Reynolds number range. The VIV  
53 behaviour will further transform if the structure oscillates and interacts with  
54 the fluid wakes, depending on several fluid-structure parameters.

## 55 **2. Experimental arrangement**

56 Experiments have been carried out in the Circulating Water Channel  
57 of the NDF (Fluids and Dynamics Research Group) at the University of

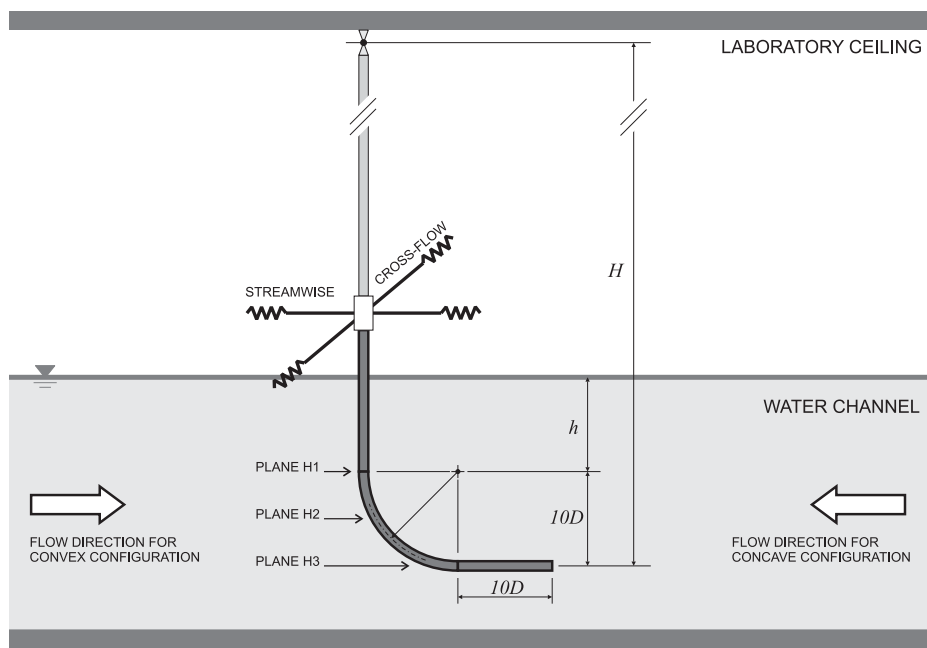


Figure 1: Experimental arrangement in the NDF-USP circulating water channel. The cylinder was rotated by 180 degrees to arrange concave and convex configurations.

58 São Paulo, Brazil. The NDF-USP water channel has an open test section  
59 0.7m wide, 0.9m deep and 7.5m long. Good quality flow can be achieved  
60 up to 1.0m/s with turbulence intensity less than 3%. This laboratory has  
61 been especially designed for experiments in flow-induced vibrations and more  
62 details about the facilities are described in Assi et al. (2006).

63 A rigid section of a curved circular cylinder, with an external diameter  
64 of  $D = 32\text{mm}$ , was made of ABS plastic and Perspex tubes according to  
65 the dimensions shown in Figure 1. The curved cylinder was composed of a  
66 horizontal section with  $10D$  in length, a curved section with a  $10D$  radius  
67 and a vertical section with length  $h/D$  that could be varied with reference  
68 to the water line. The water level was set to 700mm from the floor of the  
69 channel, which meant that the  $10D$ -long horizontal part of the cylinder was  
70 not close enough to the floor to suffer interference from the wall.

71 The model was connected by its upper end to a long pendulum rig (length  
72  $H = 3.0\text{m}$ ) that allowed the system to oscillate in two degrees of freedom  
73 (2dof) in the cross-flow and streamwise directions. The model was attached  
74 to two pairs of coil springs that provided the stiffness of the system. The  
75 springs were set to provide the same natural frequency ( $f_0$ , measured in air)  
76 in both the cross-flow and streamwise directions. The design and construction  
77 of the pendular elastic rig was made by Freire & Meneghini (2010) based  
78 on a previous idea employed by Assi et al. (2009, 2010b) for experiments  
79 with VIV suppressors. The present apparatus has been validated for VIV  
80 experiments by Freire et al. (2009, 2011).

81 Two laser sensors measured the cross-flow and streamwise displacements  
82 of the pendulum referring to the displacement of the bottom tip of the mod-  
83 els. A load cell was installed before the springs to allow for instantaneous  
84 measurements of lift and drag acting on the cylinder. (Hydrodynamic forces  
85 will not be discussed in this paper.) A particle-image velocimetry (PIV)  
86 system was employed to analyse the instantaneous wake patterns along the  
87 cylinder span.

88 Regarding the flow direction, two orientations were investigated: a con-  
89 vex and a concave configuration according to the direction of the flow ap-  
90 proaching the curvature. The flow direction in the test section of the water  
91 channel was not changed; naturally the curved cylinder was rotated by 180  
92 degrees to allow for both concave and convex arrangements. This is also  
93 illustrated in Figure 1.

94 Decay tests have been performed in air in order to determine the natural  
95 frequencies of the system in both directions as well as the level of structural  
96 damping. The apparatus with one universal joint and four springs turned  
97 out to present a very low structural damping of  $\zeta = 0.2\%$ , measured as a

Table 1: Structural properties.

	$m^*$	$\zeta$	$m^*\zeta$
Straight cylinder	2.8	0.2%	0.0056
Curved cylinders	2.1	0.2%	0.0042

98 fraction of the critical damping. The total oscillating mass of the system was  
 99 measured in air, resulting in a non-dimensional mass ratio  $m^*$ , defined as the  
 100 ratio between the total mass and the mass of displaced fluid. Consequently,  
 101 the mass-damping parameter  $m^*\zeta$  of the system was kept to the lowest  
 102 possible value in order to amplify the amplitude of response.

103 Table 1 presents a summary of the structural parameter for both the  
 104 straight and curved cylinder.

### 105 3. Results for a straight cylinder

106 A preliminary VIV experiment was performed with a straight cylinder  
 107 in order to validate the set-up and generate data for comparison. The same  
 108 pendulum rig was employed, only replacing the curved model by a straight  
 109 cylinder with the same diameter. This time, the straight cylinder was long  
 110 enough to reach the bottom wall only leaving a 3mm clearance to allow for  
 111 free movement of the pendulum in any direction.

112 The dynamic response of the straight cylinder covered a reduced velocity  
 113 range from 1.5 to 12, where reduced velocity ( $U/Df_0$ ) is defined using the  
 114 cylinder natural frequency of oscillation measured in air. The only flow  
 115 variable changed during the course of the experiments was the flow velocity  
 116  $U$ , which, as for full-scale risers, alters both the reduced velocity and the  
 117 Reynolds number between 750 and 15,000 for a maximum reduced velocity  
 118 of 20.

119 The flow around a smooth, straight circular cylinder in the considered  
 120 Reynolds number range (identified as sub-critical) is generally expected to  
 121 be three-dimensional, with a laminar boundary layer over the cylinder sur-  
 122 face and turbulent vortex wake. However, in the case of curved cylinder,  
 123 the curvature plays a significant role in modifying the wake dynamics, which  
 124 depends on the leading geometry facing the approaching flow. This entails  
 125 both the normal and axial flow components along the cylinder curved sec-  
 126 tion, further complicating the spatio-temporal vortex shedding mechanisms,  
 127 associated forces and frequencies. This has been exemplified by Miliou et  
 128 al. (2007) for  $Re = 500$ .

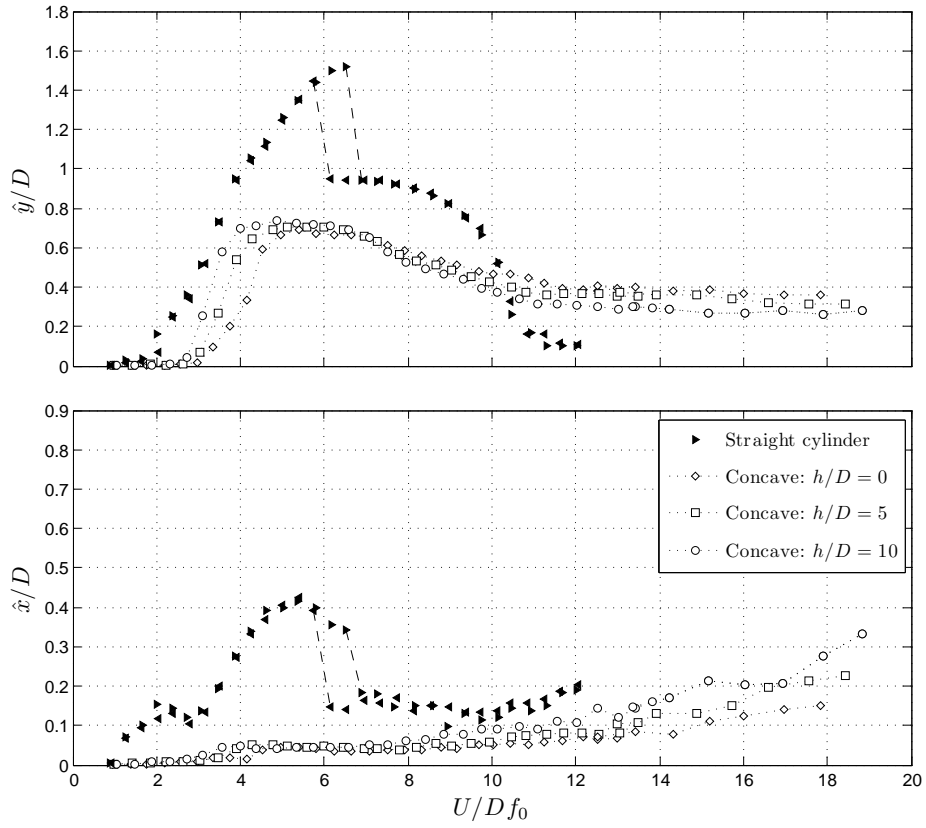


Figure 2: Cross-flow ( $\hat{y}/D$ ) and streamwise ( $\hat{x}/D$ ) amplitude of vibration versus reduced velocity for a straight cylinder and concave configurations varying the vertical section length ( $h/D$ ). Symbols  $\blacktriangleright$  are for runs with increasing flow speed, while  $\blacktriangleleft$  are for decreasing.



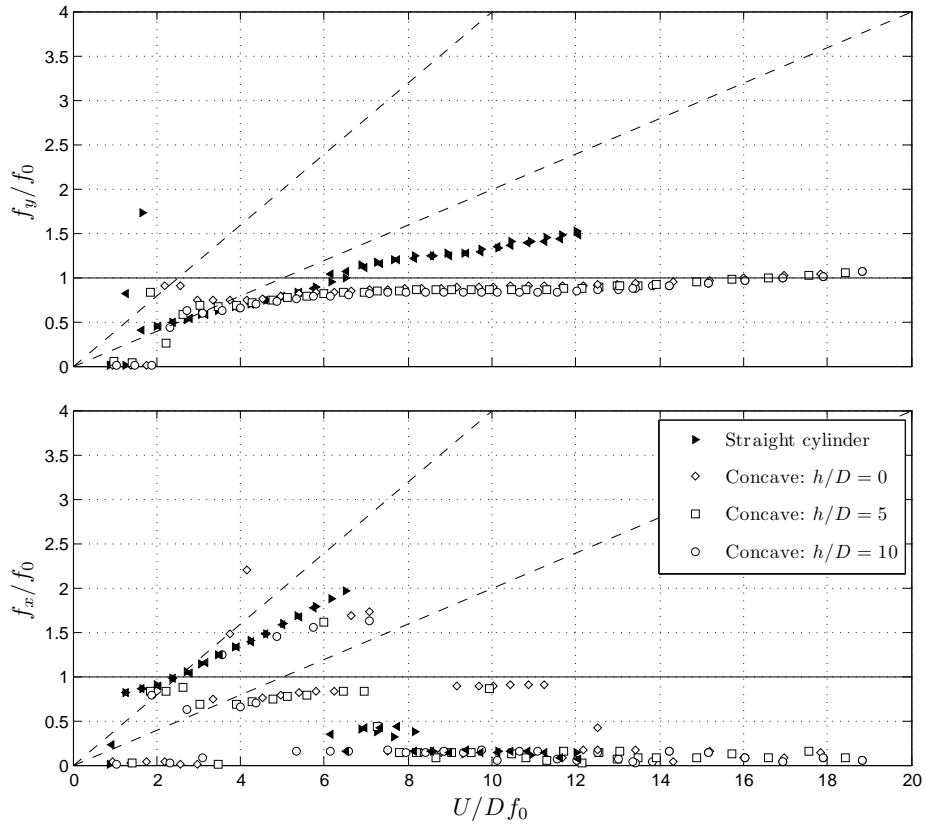


Figure 3: Cross-flow ( $\hat{y}/D$ ) and streamwise ( $\hat{x}/D$ ) dominant frequency of response versus reduced velocity for a straight cylinder and curved concave configurations varying the vertical section length ( $h/D$ ). Symbols  $\blacktriangleright$  are for runs with increasing flow speed, while  $\blacktriangleleft$  are for decreasing.

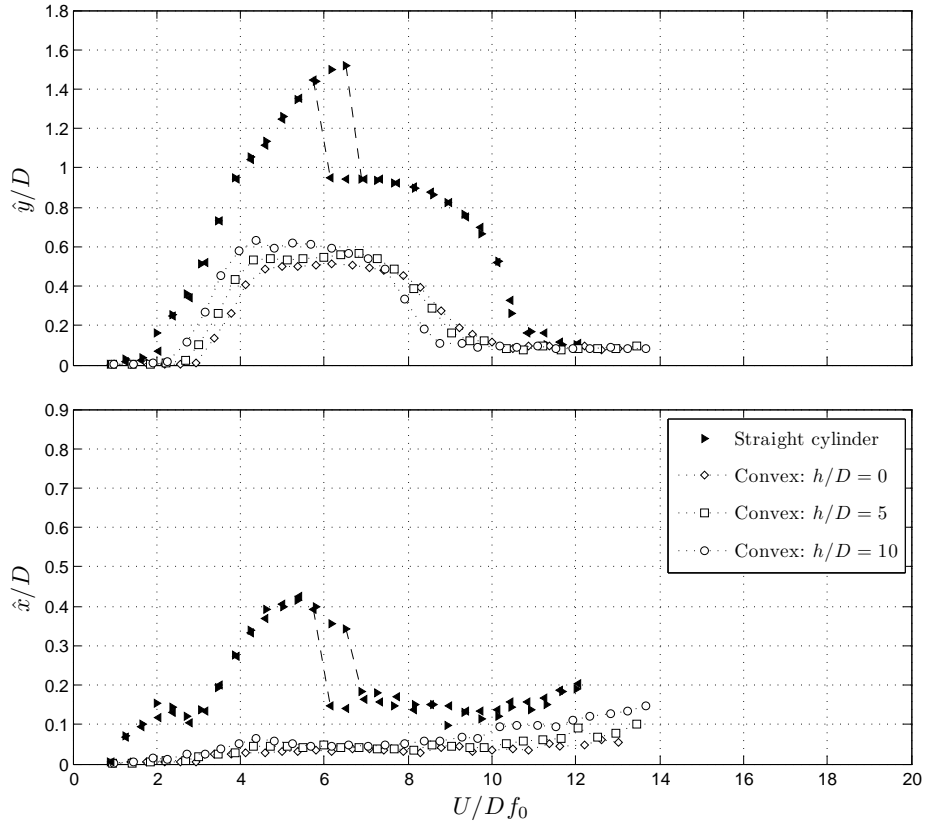


Figure 4: Cross-flow ( $\hat{y}/D$ ) and streamwise ( $\hat{x}/D$ ) amplitude of vibration versus reduced velocity for a straight cylinder and convex configurations varying the vertical section length ( $h/D$ ). Symbols  $\blacktriangleright$  are for runs with increasing flow speed, while  $\blacktriangleleft$  are for decreasing.

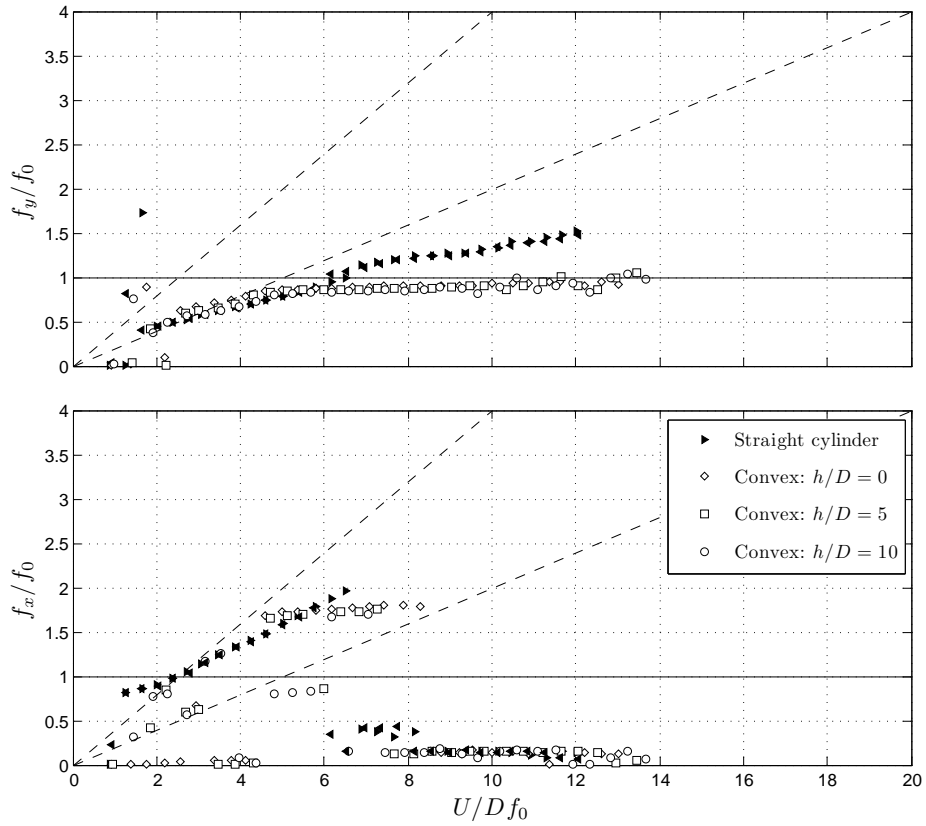


Figure 5: Cross-flow ( $\hat{y}/D$ ) and streamwise ( $\hat{x}/D$ ) dominant frequency of response versus reduced velocity for a straight cylinder and curved convex configurations varying the vertical section length ( $h/D$ ). Symbols ► are for runs with increasing flow speed, while ◄ are for decreasing.

129 Throughout the study, cylinder displacement amplitudes ( $\hat{x}/D$  for the  
130 streamwise and  $\hat{y}/D$  for the cross-flow directions) were found by measuring  
131 the root mean square value of response and multiplying by the square root  
132 of 2 (the so called harmonic amplitude). This is likely to give an underes-  
133 timation of maximum response but was judged to be perfectly acceptable  
134 for assessing the general behaviour of VIV, since the response is mostly  
135 harmonic. Results presented in the present study correspond to the dis-  
136 placement of the lowest point of the model, i.e., the end of the cylinder  
137 closer to the section floor, thus representing the maximum displacement de-  
138 veloped by each model. Consequently, the equivalent amplitude at the water  
139 surface for the cylinder with a  $10D$  vertical section is 20% smaller than the  
140 amplitude indicated in the results. Applying similar corrections, amplitudes  
141 are 16% smaller for the cylinder with a  $5D$  vertical section and 11% smaller  
142 for the cylinder with no vertical section.

143 Displacements are non-dimensionalised by the cylinder diameter  $D$ . The  
144 dataset for the straight cylinder is repeated in Figures 2 to 5 to serve as  
145 reference.

146 Figures 2 and 4 compare the reference cross-flow and streamwise re-  
147 sponses obtained from two different runs with the straight cylinder. In the  
148 first one, the flow speed ( $U$ ) was increased in 30 steps from zero to a maxi-  
149 mum, while in the second it was decreased from the maximum to zero. Both  
150 data sets overlap rather well for all the reduced velocity range except for a  
151 region around  $U/Df_0 = 6$  where the well-known phenomenon of hysteresis  
152 in the VIV response has been observed. The streamwise VIV response also  
153 seems to occur in two resonance ranges ( $U/Df_0 = 2$  and  $6$ ), the so-called  
154 second and third instability ranges involving asymmetric vortices (Bearman,  
155 1984).

156 Although the observed peak amplitude of  $\hat{y}/D = 1.5$  around  $U/Df_0 = 6$   
157 is slightly higher than other results found in the literature for similar values  
158 of  $m^*\zeta$  (for example, Assi et al., 2009) the general behaviour of both curves  
159 show a typical response for 2-dof VIV. The higher amplitude found here  
160 could be explained by the very low mass-damping characteristics of the  
161 system and the geometric projection of the amplitude at the tip of the  
162 model and not at mid-length as usual.

163 Although the cylinder was initially aligned in the vertical position, in  
164 flowing water the mean drag displaces the cylinder from its original location  
165 reaching a slightly inclined configuration from the vertical. This was judged  
166 not to be detrimental to the experiment; hence the inclination of the cylinder  
167 was not corrected between each step. The same procedure was adopted for  
168 the curved cylinder.

169 Figures 3 and 5 present the dominant frequency of response versus re-  
 170 duced velocity. Two dashed lines inclined with different slopes represent the  
 171 region for a Strouhal number of 0.2 and 0.4, i.e., an estimation of the vortex  
 172 shedding frequency for a straight cylinder in the cross-flow and streamwise  
 173 direction respectively. It is clear that the straight cylinder presents a typical  
 174 VIV response oscillating in the cross-flow direction with a frequency follow-  
 175 ing the  $St = 0.2$  line up to the beginning of the upper branch. Eventually,  
 176  $f_y/f_0$  departs from  $St = 0.2$  towards the unity value around  $U/Df_0 = 6$ .  
 177 The behaviour observed for the streamwise vibration is also typical of VIV  
 178 with the difference that the frequency of response is twice as that for the  
 179 cross-flow direction during much of the synchronisation range.

#### 180 4. Response of the curved cylinder

181 As mentioned above, experiments with the curved cylinder were per-  
 182 formed taking into account two distinct configurations as far as the flow  
 183 direction is concerned. In the concave configuration the flow approaches the  
 184 model reaching first the horizontal section. As opposed to that, in the con-  
 185 vex configuration the horizontal section is placed downstream of the curved  
 186 and vertical parts.

##### 187 4.1. Amplitude of vibration

188 In general terms, as presented in Figures 2 and 4, the curved cylinders  
 189 showed significantly less vibration for both concave and convex configura-  
 190 tions when compared to the typical VIV response of the straight cylinder.  
 191 Such a reduction is noticeable in both the cross-flow and streamwise re-  
 192 sponses. This clearly shows that the curvature of the cylinder modifies the  
 193 vortex shedding mechanism in a manner that the structure extracts less en-  
 194 ergy from the flow. We shall return to this point when investigating the  
 195 velocity flow field with PIV.

196 For each concave and convex configuration, the vertical section of the  
 197 cylinder close to the free surface was varied in three different lengths:  $h/D =$   
 198 0, 5 and 10. The overall response for the three values of  $h/D$  is very similar,  
 199 showing only minor differences at the beginning of the synchronisation range  
 200 between  $U/Df_0 = 3.0$  and 5.0. Apart from that, no distinct behaviour was  
 201 observed as far as a variation in  $h/D$  is concerned for both concave and  
 202 convex configurations.

203 The cross-flow displacement does not reveal distinct upper and lower  
 204 branches of vibration such as those observed for a straight cylinder, but it  
 205 produces a smooth curve that spans the whole synchronisation region with

206 maximum amplitude around  $\hat{y}/D = 0.75$  for the concave and 0.65 for the  
207 convex configurations. No hysteresis is found.

208 However, the most interesting feature of such a behaviour is found when  
209 the convex response is compared to the concave one (Figures 2 and 4). While  
210 the convex curve for  $\hat{y}/D$  drops immediately between  $U/Df_0 = 8$  and 10 to a  
211 level of  $\hat{y}/D \approx 0.1$ , the response for the concave case does not diminish, but is  
212 sustained for higher reduced velocities around  $\hat{y}/D = 0.3$  until the end of the  
213 experiment. Apparently there must be a fluid-elastic mechanism occurring  
214 for reduced velocities above 8.0 for the concave configuration capable of  
215 extracting energy from the flow to sustain vibrations around  $\hat{y}/D = 0.3$ .  
216 We shall discuss this point later while analysing the PIV flow fields.

217 In the streamwise direction the responses of the curved cylinders are dif-  
218 ferent from the typical VIV developed by the straight cylinder. Streamwise  
219 vibrations in the first and second resonance regions are totally suppressed,  
220 probably owing to the hydrodynamic damping effect induced by the cylin-  
221 der's horizontal part. At the same time, the streamwise vibration  $\hat{x}/D$  for  
222 the concave case also shows increasing amplitude beginning at reduced ve-  
223 locities higher than 10 and reaching  $\hat{x}/D \approx 0.35$  for the highest flow speed.  
224 It coincides with the increased amplitude observed in the cross-flow direc-  
225 tion and should be related to the same excitation mechanism. Once more,  
226 no distinct difference in the streamwise response was observed while varying  
227  $h/D$ .

#### 228 4.2. Frequency of vibration

229 Figures 3 and 5 present the dominant frequency of oscillation non-dimensionalised  
230 by the natural frequency for both cross-flow and streamwise directions of  
231 motion. Results for the curved cylinder show a consistent behaviour in the  
232 cross-flow direction, with data points following the Strouhal line up to the  
233 upper branch peak but remaining closer to  $f_y/f_0 = 1.0$  for the rest of the  
234 reduced velocity range. In the streamwise direction, we find data points fol-  
235 lowing both Strouhal lines and also very low frequencies indicating random  
236 drifts instead of periodic oscillations. Since the displacements in the stream-  
237 wise direction are much smaller for the curved cylinder than the straight one,  
238 we should expect broader frequency spectra dominating over the response.

239 One might remember that the straight and curved cylinder should have  
240 very similar values of added mass in the cross-flow direction, but slightly  
241 different values in the streamwise direction due to the geometric properties  
242 relative to the flow. We have not taken such effect into account in this  
243 paper, but it might be playing an important role defining the frequencies of  
244 oscillation in water.

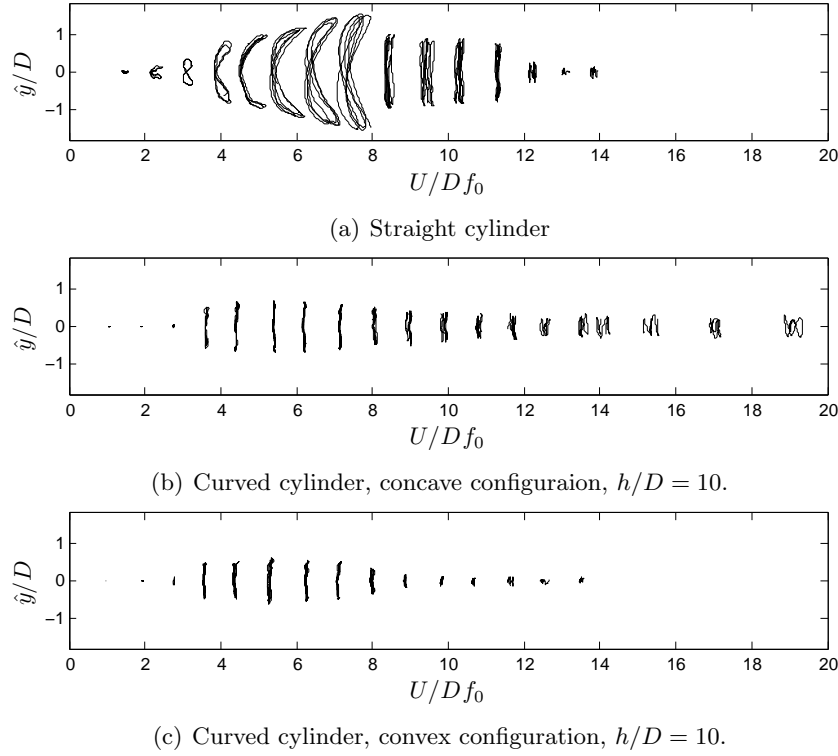


Figure 6: Response trajectories of motion for a (a) straight cylinder and a curved cylinder in (b) concave and (c) convex configurations. Each trajectory was taken at the reduced velocity indicated in the horizontal axis.

#### 245 4.3. Trajectories of motion

246 Figure 6 qualitatively compares samples of displacement trajectories ob-  
 247 tained for three experiments performed with the straight cylinder and the  
 248 curved cylinders with  $h/D = 10$ . The straight cylinder presents distinct  
 249 eight-shape figures typical of 2dof VIV owing to the 2:1 ratio on the stream-  
 250 wise to cross-flow frequency of excitation. On the other hand, trajectories  
 251 for both configurations of the curved cylinder reveal that the streamwise  
 252 displacement is greatly reduced when compared to the straight cylinder.  
 253 Both concave and convex cases show very little movement in the streamwise  
 254 direction for the whole range of reduced velocity.

255 Another interesting observation relates to the movement of both curved  
 256 cylinders. It is clear that for reduced velocities greater than 10 the convex  
 257 cylinder shows small displacements in both directions, while vibrations are  
 258 sustained until the end of the experiment for the concave case as shown in

259 Figures 2 and 4.

## 260 **5. Velocity and vorticity fields of stationary cylinders**

261 Two dimensional PIV (particle image velocimetry) measurements of the  
262 flow around the cylinder were performed, for both concave and convex con-  
263 figurations, on a vertical plane parallel to the plane of curvature. In addition,  
264 PIV measurements were also performed on three horizontal planes (marked  
265 H1, H2 and H3 in Figure 1 across the cylinder diameter.

266 All PIV measurements were taken for  $Re = 1000$  in the sub-critical  
267 Reynolds number regime found for a straight circular cylinder. According  
268 to Williamson (1996), the particular flow is in the shear-layer transition  
269 regime, characterised by an increase on the base suction, a gradual decrease  
270 in the Strouhal number and a decrease in the formation length of the mean  
271 recirculation region. These trends are caused by the developing instability  
272 of the separating shear layers from the sides of the body. The flow around  
273 a curved cylinder, which presents different elliptical cross-sections along the  
274 span, may behave slightly different from the above description. Further  
275 investigation is necessary in order to evaluate that.

### 276 *5.1. Vertical plane*

277 We shall start discussing the results obtained from the vertical plane, as  
278 presented in Figures 7 to 12. Four visualisation areas for each configuration,  
279 labelled A1 to A4, were conveniently distributed along the length of the  
280 cylinder in order to evaluate as much as possible to the flow pattern around  
281 the body. All four areas are in the same plane illuminated by the laser,  
282 which is parallel to the plane of curvature only dislocated by  $1D$  from the  
283 centre of the cylinder towards the camera in order to capture the highest  
284 velocities induced by the vortex tubes. Figures 9 and 12 show the location  
285 of each area composing the flow field along the cylinder. It is important  
286 to note that each velocity field was obtained from a different acquisition  
287 instant; hence A1, A2, A3 and A4 are not correlated in time.

288 All PIV measurements were performed for a static cylinder at  $Re \approx 1000$ .  
289 Of course the wake pattern for the static cylinder is expected to be different  
290 from the wake of an oscillating cylinder, but even an analysis of a fixed  
291 body can contribute to the understanding of the complex vortex-structure  
292 interaction occurring during the response. A similar approach was employed  
293 by Miliou et al. (2007) who performed numerical simulations for a static,  
294 curved cylinder between  $Re = 100$  and  $500$ . The same colour scales have



295 been employed from Figures 7 to 12 to allow for direct comparison of velocity  
296 magnitude and vorticity contours.

297 With that in mind, let us analyse first the flow pattern around the concave  
298 configuration in Figures 7 to 9. The overall flow around the body can  
299 be divided in two parts:

300 (I) Areas A1 and A2 show the region where the flow is mostly parallel to  
301 the axis of the cylinder. Therefore, no clear vortex tubes are observed with  
302 concentrated axial vorticity. Instead, the flow along the horizontal length is  
303 disturbed by the separation occurring at the tip of the cylinder. Area A1  
304 shows the flow approaching the disk facing upstream and separating into a  
305 recirculation bubble. The periodicity of the shedding associated with this  
306 region is also related to the flow speed and the diameter  $D$ , but no coherent  
307 vortices parallel to the cylinder are able to form. As a consequence, a cascade  
308 of small vortices is convected downstream along the horizontal length (see  
309 area A2) reaching the beginning of the curved section.

310 (II) Areas A3 and A4 show the region where the flow is mainly perpen-  
311 dicular to the axis of the cylinder. Coherent vortex tubes tend to form fol-  
312 lowing the curvature of the body, but further downstream they are stretched  
313 and rapidly breakdown into smaller vortices that are convected by the flow.  
314 Area A3 shows the instant when a vortex tube is shed almost tangent to  
315 the curvature, while area A4, around the vertical section, reveal a formation  
316 region more or less aligned with the axis of the cylinder. Streamlines drawn  
317 in areas A3 and A4 reveal a non-negligible velocity component deflecting  
318 the flow downwards immediately after the vortex formation region. As we  
319 move along the cylinder towards the water line from A3 to A4 the down-  
320 ward component is gradually reduced until it eventually disappears towards  
321 the upper half of A4. This region marks the competition between two wake  
322 modes existent along the transition from curved to straight cylinder. This  
323 looks similar to Figure 15 in Miliou et al. (2007), with  $Re = 100$ , although  
324 without the cylinder horizontal section therein.

325 Analysing the flow pattern for the convex configuration in Figures 10 to  
326 12 we notice two striking differences:

327 Firstly, because the flow approaching the convex body does not encounter  
328 a blunt disk facing upstream, no strong separation or recirculation bubble  
329 is formed. As a consequence, the horizontal section seen in areas A1 and  
330 A2 is not exposed to a disturbed, unsteady flow parallel to the axis of the  
331 cylinder. In fact, A1 and A2 reveal that the upper half of the horizontal  
332 length is exposed to a periodic flow formed by a regular wake, while the  
333 bottom half experiences almost no perturbation, with streamlines showing  
334 a well behaved flow field parallel to the axis.

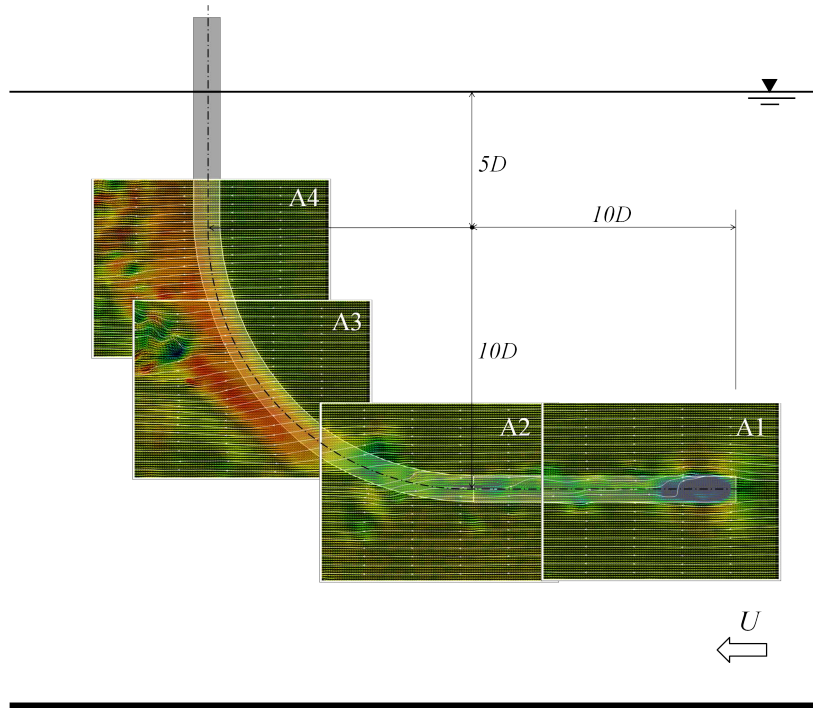


Figure 7: Composition of instantaneous PIV velocity fields for concave configuration with  $h/D = 5$ .

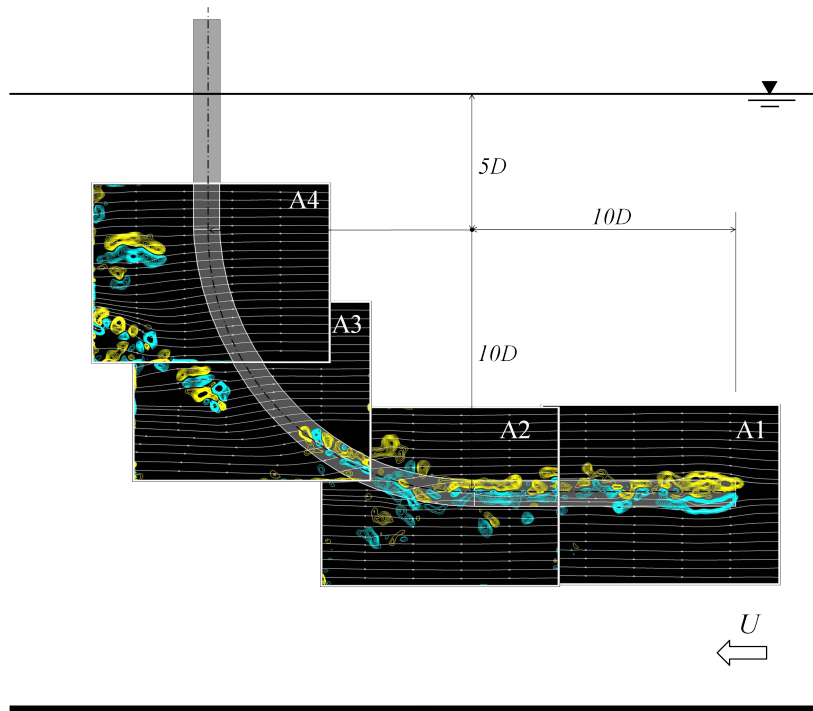


Figure 8: Composition of instantaneous PIV vorticity fields for concave configuration with  $h/D = 5$ .

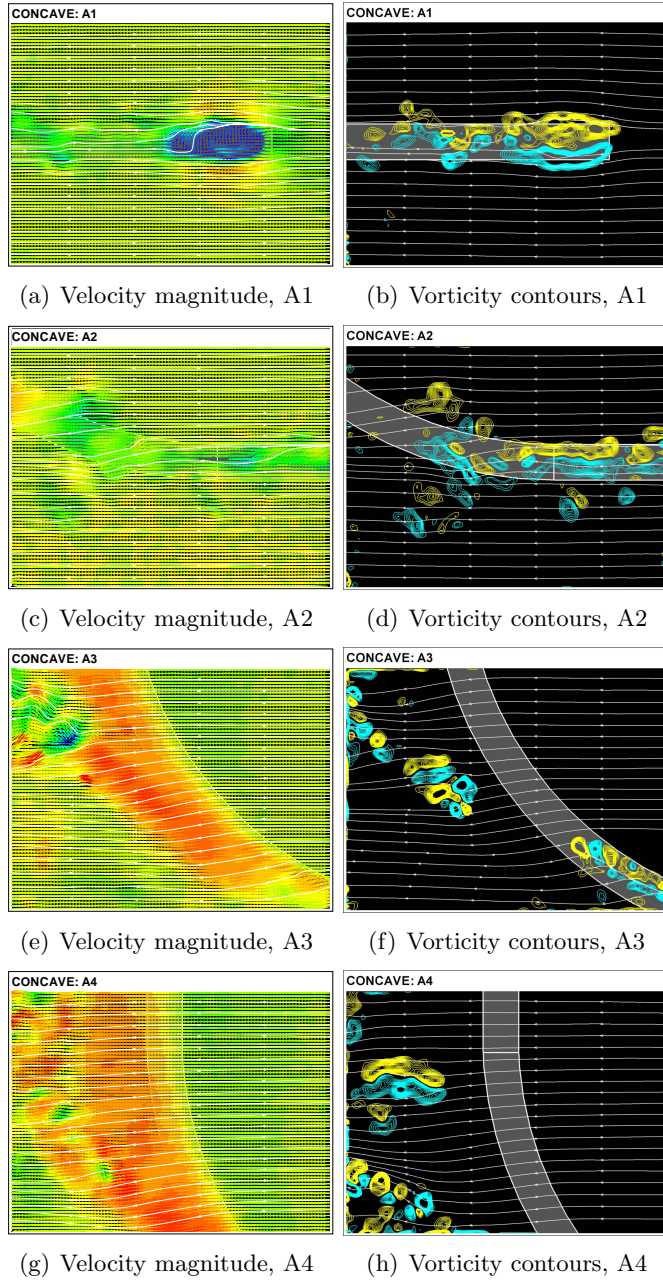


Figure 9: Detailed velocity and vorticity fields from Figures 7 and 8. Flow direction is from right to left.  $Re = 1000$ . Colour scale for velocity magnitude is from  $0.004\text{m/s}$  (blue) to  $0.05\text{m/s}$  (red). Colour scale for vorticity contours is in the range  $\pm 0.004\text{s}^{-1}$ . (Velocity fields do not correspond to the vorticity fields in time.)

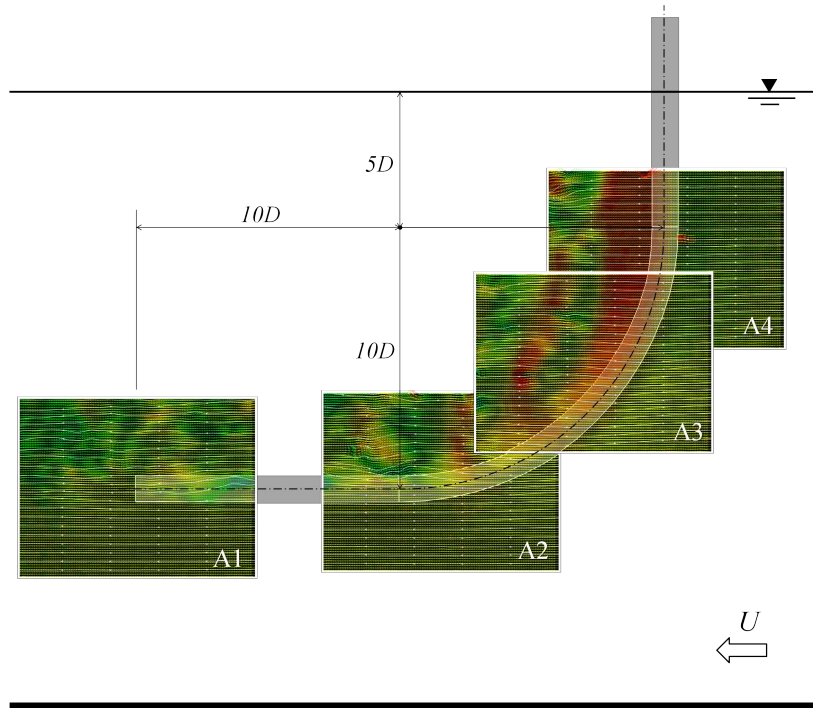


Figure 10: Composition of instantaneous PIV velocity fields for convex configuration with  $h/D = 5$ .

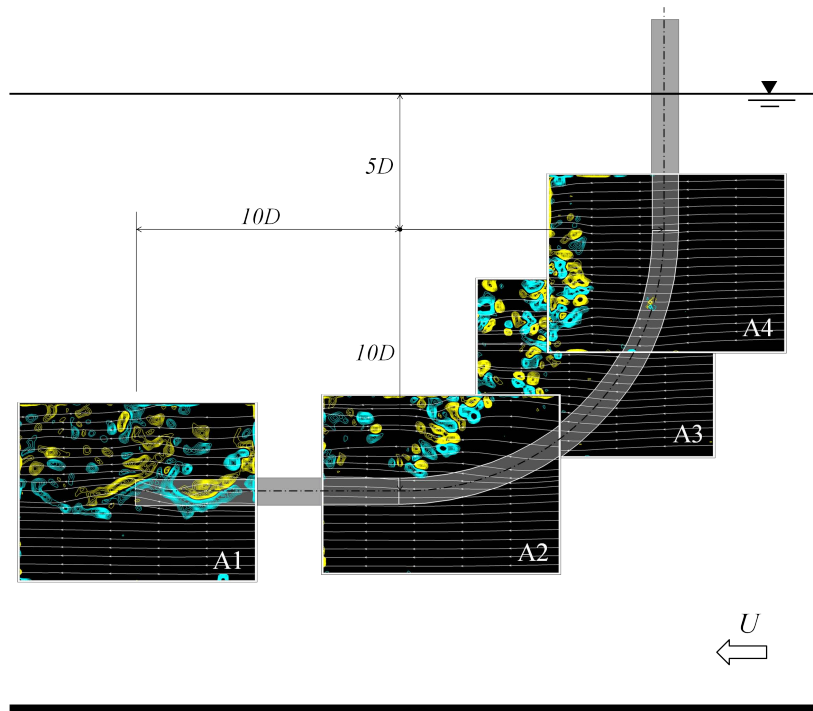


Figure 11: Composition of instantaneous PIV vorticity fields for convex configuration with  $h/D = 5$ .

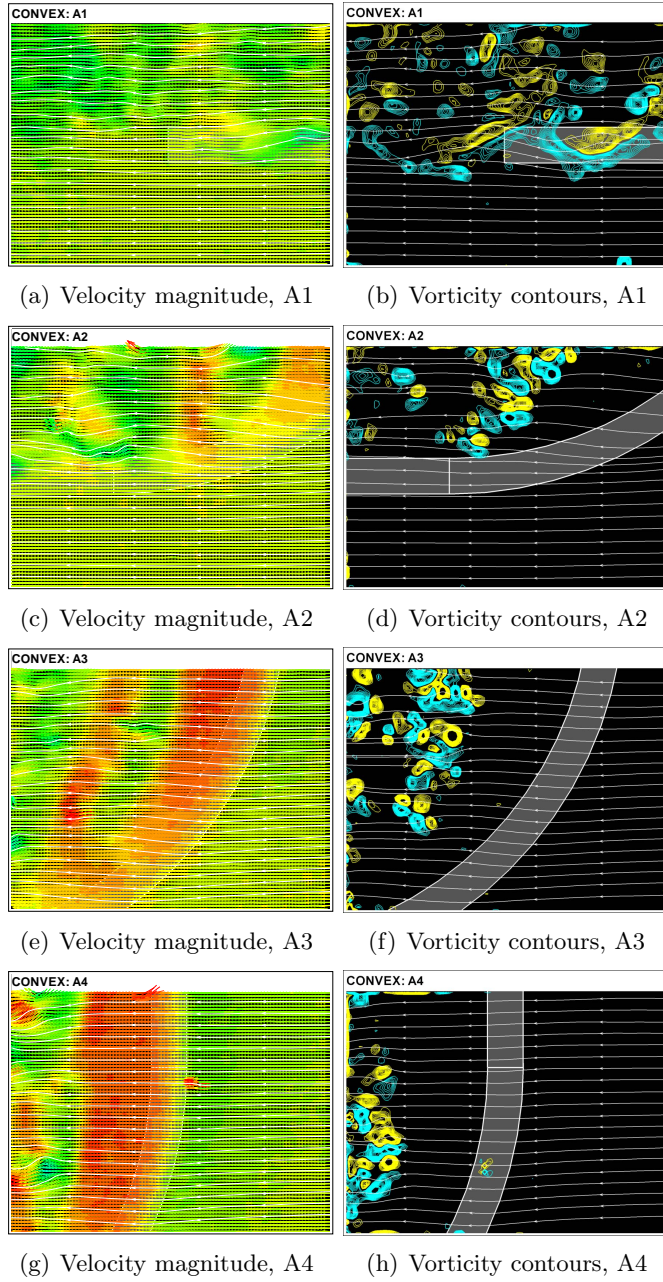


Figure 12: Detailed velocity and vorticity fields from Figures 10 and 11. Flow direction is from right to left.  $Re = 1000$ . Colour scale for velocity magnitude is from  $0.004\text{m/s}$  (blue) to  $0.05\text{m/s}$  (red). Colour scale for vorticity contours is in the range  $\pm 0,004\text{s}^{-1}$ . (Velocity fields do not correspond to the vorticity fields in time.)

335 Secondly, looking at the upper half of the body (A3 and A4) we notice  
336 much stronger and coherent vortex tubes when compared to the flow around  
337 the concave configuration. Area A3 reveals some kind of vortex dislocation  
338 after a formation region that increases in length as we move upwards. Be-  
339 cause the convex geometry does not encourage the vortex tubes to stretch  
340 and break, a periodic wake seems to be sustained farther downstream. In  
341 contrast with the flow around the concave configuration, the velocity field  
342 around the curved section has a non-negligible vertical component upwards.  
343 It is stronger in A2 and is gradually reduced as we move upwards along the  
344 curvature in A3. This looks similar to Figure 3 in Miliou et al. (2007) for  
345  $Re = 100$ .

346 Gallardo et al. (2011) stated that there is a certain degree of alignment  
347 of the flow structures with the axial curvature of the cylinder, which tilts  
348 the flow structures with respect to the vertical direction. Figures 12(e) and  
349 12(f) capture this behaviour, also recognised in Figure 2 of Gallardo et al.  
350 (2011) and Figure 8 of Miliou et al. (2007).

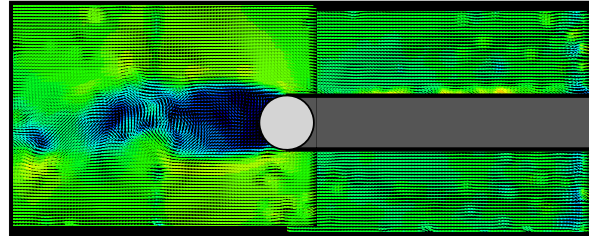
## 351 5.2. Horizontal planes

352 Figures 13 and 14 present PIV velocity fields for the three horizontal  
353 planes indicated by H1, H2 and H3 in Figure 1. All measurements were  
354 performed with  $h/D = 5$ . Plane H1 was positioned at the transition from  
355 the straight to the curved section of the model, i.e.,  $5D$  below the water  
356 line. Plane H2 was located  $5D$  below that position and plane H3 another  
357  $5D$  down towards the floor.

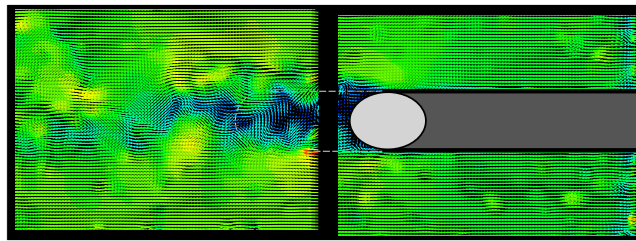
358 Figure 13 presents results for the concave configuration. The two cam-  
359 eras were positioned underneath the model as viewing from the bottom  
360 through the glass floor. A light grey circle or ellipse marks the cross section  
361 of the cylinder at the illuminated plane. A dark grey rectangle represents  
362 the part of the curved model in front of the laser plane, while a dashed line  
363 illustrates the projection of the model behind the plane. Each image is com-  
364 posed of two PIV areas taken simultaneously; for some cases they overlap,  
365 for others they are apart.

366 In Figure 13(a), for the horizontal plane at the transition from the  
367 straight to the curved section, we notice a wider wake with a longer for-  
368 mation region that generates stronger vortices. This formation is related  
369 to the strong vortex tubes parallel to the straight section presented in Fig-  
370 ure 9(g). Moving down to plane H2, the cross section of the cylinder turns  
371 into an ellipse. The wake becomes much narrower with a short formation  
372 length and no strong vortices are distinguishable in the downstream flow.  
373 Figure 9(e) also showed that an oblique vortex tube would form closer to

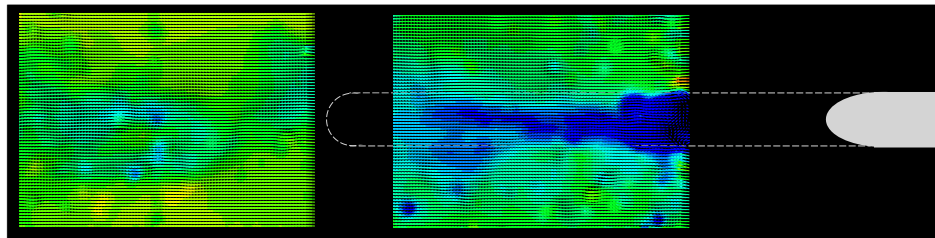




(a) Plane H1

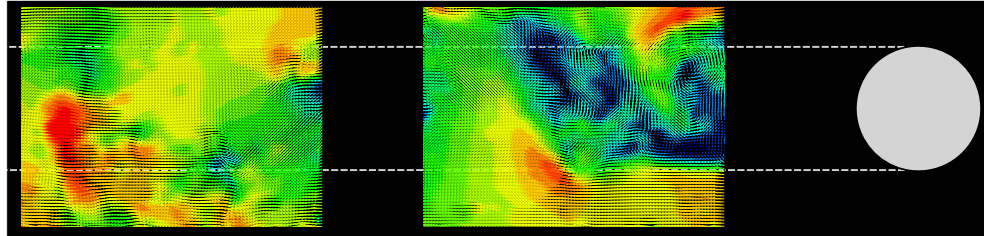


(b) Plane H2

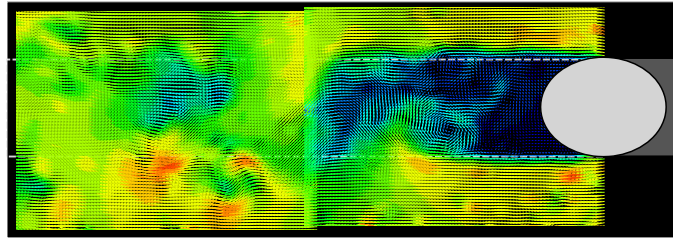


(c) Plane H3

Figure 13: Velocity fields for horizontal planes across the concave configuration. Please refer to Figure 1 for positions. Flow direction is from right to left.  $Re = 1000$ . Colour scale for velocity magnitude is from 0.004m/s (blue) to 0.05m/s (red).



(a) Plane H1



(b) Plane H2

Figure 14: Velocity fields for horizontal planes across the convex configuration. Please refer to Figure 1 for positions. Flow direction is from right to left.  $Re = 1000$ . Colour scale for velocity magnitude is from  $0.004\text{m/s}$  (blue) to  $0.05\text{m/s}$  (red).

374 the cylinder with vortices breaking apart into smaller eddies. Farther down  
 375 to plane H3, the cross section illuminated by the laser plane now shows the  
 376 beginning of the horizontal portion of the model. No vortex wake is iden-  
 377 tified, but only a region of disturbed flow which agrees with pattern shown  
 378 in Figure 9(c).

379 Results for the convex configuration in Figure 14 were obtained in the  
 380 same way as the concave, the only difference being that the cameras were  
 381 installed above the channel, viewing from the top through the free surface.  
 382 As a consequence, plane H3 does not result in any useful velocity field once  
 383 the flow that separates from the cylinder follows attached to the horizontal  
 384 portion of the model, as seen in Figure 12(c).

385 Figure 14(a) presents velocity fields for the the first plane H1 at the  
 386 transition region. A rather wide wake with strong vortical structures is  
 387 noticeable through high induced velocities. Again, the same pattern was  
 388 captured on the vertical PIV shown in Figure 12(g). Moving down to plane  
 389 H2 we notice that an organised wake may still exist, even though the cross  
 390 section of the cylinder turned into an ellipse. Vortex tubes were also ver-  
 391 ified to persist further downstream in Figures 12(c) and 12(e) as coherent  
 392 flow structures appeared periodically downstream of the cylinder in the flow



393 fields. Similar vortex structures were verified by Miliou et al. (2007) and  
394 Gallardo et al. (2011). This proves that the convex configuration is more  
395 prone to produce correlated vortex tubes along the curved length of the  
396 cylinder, while in the concave configuration vortices soon break apart as  
397 they are convected downstream.

398 Based on the results of Gallardo et al. (2011) for the convex configu-  
399 ration, one can observe that the interaction of the shear layers and thus  
400 the vortex formation length is a function of the cross-sectional shape being  
401 circular or elliptical, here represented by different planes along the cylinder  
402 span as can be seen in Figure 14 and also in Figure 3 of Gallardo et al.  
403 (2011).

404 Plane H1 in Figure 14(a), which corresponds to plane  $z/D = 16$  in  
405 Gallardo et al. (2011), shows that the shear layers interact in a farther  
406 downstream position from the body and the wake is wider compared to a  
407 horizontal position of the H2 plane in Figure 14(b) where the cross-section of  
408 the cylinder is elliptical. In the latter case, seen also at the  $z/D = 8$  plane in  
409 Gallardo et al. (2011), there are vortices produced within the recirculation  
410 region exhibiting the wavier shear layers.

## 411 6. The excitation mechanism

412 The main question to be answered by the present study is concerned  
413 with the fact that the amplitude in the cross-flow direction for the convex  
414 configuration is able to drop down to 0.1 for high reduced velocities while  
415 the concave configuration sustains vibration around 0.35. We believe this  
416 distinct behaviour between the convex and the concave configurations is  
417 related to the wake interference happening in the lower half of the cylinder  
418 due to perturbations generated in the horizontal section when it is positioned  
419 upstream.

420 In the concave configuration the horizontal part of the cylinder is located  
421 upstream of the curved and vertical parts. The approaching flow encoun-  
422 ters a circular blunt leading edge with a clear separation region around the  
423 circumference (Figure 9(a)). The flow that separates at the leading edge  
424 tends to create a separation bubble and latter reattaches along the horizon-  
425 tal section of the cylinder. Because the cylinder already presents cross-flow  
426 and streamwise vibrations, the three-dimensional separation bubble will not  
427 find a stable configuration nor a definite reattachment region, instead it will  
428 develop a periodic behaviour that may result in three-dimensional vortices  
429 being shed downstream, reaching the other parts of the cylinder. This is  
430 very clear in areas A1 and A2 of Figures 7 and 9 for the static cylinder.

431 The fluid-elastic mechanism behind the response may be a composition  
432 of different phenomena acting at the same time. We believe this interac-  
433 tion between the disturbed flow from the upstream horizontal part with the  
434 curved and vertical parts is responsible for sustaining the level of vibration  
435 around  $\hat{y}/D = 0.35$  and  $\hat{x}/D = 0.35$ . We suggest such an interaction may  
436 be occurring in the following forms:

437 (i) Vortices generated along the horizontal section may impinge on the  
438 curved part generating impulses in the same manner that large eddies of  
439 turbulence induce buffeting on elastic structures. Because the concave con-  
440 figuration has a longer section immersed in such a disturbed wake it is more  
441 susceptible to buffet. Evidence that a buffeting-like phenomenon might be  
442 occurring is that the streamwise vibration shows a considerable increase  
443 in amplitude with increasing flow speed further out of the synchronisation  
444 range. Figure 6(b) also reveals that these vibrations are not harmonic and  
445 may even be chaotic, another evidence supporting the buffeting-excitation  
446 hypothesis.

447 (ii) The disturbed flow from the horizontal part may be disturbing and  
448 disrupting the vortex shedding mechanism from the curved and vertical sec-  
449 tions, for example uncorrelating the vortex shedding mechanism in a curved  
450 region of the cylinder near the horizontal part. Also, the vortex wake along  
451 the curved-vertical half of the concave cylinder showed less correlation along  
452 the span, resulting in a lower peak of vibration during the synchronisation  
453 range.

454 (iii) Because the concave configuration has a fixed separation ring at the  
455 circle facing upstream, there might be some galloping-like instability related  
456 to the separation and reattachment of the three-dimensional bubble. This  
457 could generate non-resonant forces that could sustain some level of vibration  
458 for reduced velocities above the synchronisation range.

459 (iv) Finally, the concave configuration might experience some kind of  
460 instability related to the geometric arrangement of the experiment. Because  
461 the centre of pressure is located upstream of the vertical axis of the pendulum  
462 a minute deflection of the cylinder may result in a resolved force that will  
463 increase displacement. The opposite is true for the convex configuration in  
464 which the centre of pressure downstream of the vertical axis of the pendulum  
465 can only generate stabilising forces.

466 Of course all four mechanisms suggested above may also be occurring  
467 simultaneously or it may not even be possible to explain them separately.  
468 In addition, they might as well be very dependent on Reynolds number and  
469 amplitude of vibration.

470 **7. Conclusions**

471 We have experimentally investigated the two-degree-of-freedom VIV re-  
472 sponse of a rigid, curved circular cylinder with a low mass-damping ratio.  
473 With regard to the approaching flow (Reynolds number is in the range of  
474 750-15,000) both concave and convex configurations were considered and the  
475 measured responses were compared with those of a typical straight cylinder.  
476 In summary, we conclude that:

477 (i) In general terms, a curved cylinder presents a lower peak of amplitude  
478 of vibration in both the cross-flow and streamwise direction when compared  
479 to a straight cylinder. Nevertheless, a considerable level of streamwise vi-  
480 bration, not attributed to VIV, was observed for reduced velocity as high as  
481 18.

482 (ii) Although the peak amplitude is reduced, a curved cylinder may  
483 present a significant level of vibration that is sustained for higher values of  
484 reduced velocity beyond the end of the typical synchronisation range.

485 (iii) The concave configuration shows a considerable level of cross-flow  
486 vibration around  $\hat{y}/d = 0.35$  up to the highest reduced velocity performed  
487 in this experiment.

488 (iv) The overall response showed little dependency on the vertical length  
489 immediately below the water line, at least for a section varying between  
490  $h/D = 0$  and 10.

491 (v) From the PIV study on a stationary curved cylinder, we suggest  
492 that the flow-structure interaction mechanism that differentiates the concave  
493 from the convex cylinder response may have its origin in the disturbed flow  
494 that separates from the horizontal part located upstream. This could be  
495 related to buffeting, galloping, disturbed VIV or geometric instabilities.

496 Future work should concentrate on correlated PIV analyses of the vor-  
497 tex formation along the curvature as well as on measurements of the flow  
498 field on planes perpendicular to the plane of curvature. An investigation of  
499 the interference effect generated by the separation at the tip of the horizon-  
500 tal section could also help towards understanding the response. PIV and  
501 instantaneous force measurements for an oscillating cylinder, especially at  
502 high reduced velocities, could throw some light into the actual mechanism  
503 of excitation.

504 **Acknowledgements**

505 G.R.S. Assi wishes to acknowledge the support of CNPq (308916/2012-  
506 3) and FAPESP (11/00205-6). C.M. Freire acknowledges support from

507 FAPESP (10/00053-9). N. Srinil is grateful to the “Sir David Anderson  
508 Award” from the University of Strathclyde and the “Early Career Researcher  
509 International Exchange Award” supported by The Scottish Funding Council.  
510 cil.

## 511 **References**

- 512 Assi, G.R.S., Meneghini, J.R., Aranha, J.A.P., Bearman, P.W., Casaprima,  
513 E. **2006** Experimental investigation of flow-induced vibration interference  
514 between two circular cylinders. *J. Fluids and Structures*, 22, 819-827.
- 515 Assi, G.R.S., Bearman, P.W and Kitney, N **2009** Low Drag Solutions for  
516 Suppressing Vortex-Induced Vibration of Circular Cylinders. *J. Fluids and*  
517 *Structures* 25, 1-10.
- 518 Assi, G.R.S., Bearman, P.W., Meneghini, J.R. **2010** On the wake-induced  
519 vibration of tandem circular cylinders: the vortex interaction excitation  
520 mechanism *J. Fluid Mech.*, 661, 365-401.
- 521 Assi, G.R.S., Bearman, P.W., Kitney, N., Tognarelli, M.A. **2010b** Suppres-  
522 sion of Wake-Induced Vibration of Tandem Cylinders with Free-to-Rotate  
523 Control Plates. *J. Fluids and Structures*, 26, 1045-1057.
- 524 Bearman, P.W. **1984** Vortex shedding from oscillating bluff bodies. *Annu.*  
525 *Rev. Fluid Mech.*, 16, 195-222.
- 526 Freire, C.M., Korkischko, I., Meneghini, J.R. **2009** Development of an elastic  
527 base with tow degrees of freedom for VIV studies. *In the proceedings of*  
528 *COBEM 2009 – 20th International Congress of Mechanical Engineering*,  
529 2009, Gramado, Brazil.
- 530 Freire, C.M., Meneghini, J.R. **2010**. Experimental investigation of VIV on a  
531 circular cylinder mounted on an articulated elastic base with two degrees-  
532 of-freedom. *In the proceedings of BBVIV6 – IUTAM Symposium on Bluff*  
533 *Body Wakes and Vortex-Induced Vibrations*, 2010, Capri, Italy.
- 534 Freire, C.M., Korkischko, I., Meneghini, J.R. **2011** Definning a parame-  
535 ter of effectiveness for the suppression of vortex-induced vibration. *In*  
536 *the proceedings of OMAE2011 – 30th International Conference on Ocean,*  
537 *Offshore and Arctic Engineering*, 2011, Rotterdam, The Netherlands.
- 538 Gallardo, J. P., Pettersen, B., Andersson, H. I. **2011** Dynamics in the tur-  
539 bulent wake of a curved circular cylinder. *J. Phys. Conf. Ser.* 318, 062008.

- 540 Miliou, A., De Vecchi, A., Sherwin, S.J., Graham, M.R. **2007** Wake dynam-  
541 ics of external flow past a curved circular cylinder with the free stream  
542 aligned with the plane of curvature *J. Fluid Mech.*, 592, 89-115.
- 543 Srinil, N. **2010** Multi-mode interactions in vortex-induced vibrations of flex-  
544 ible curved/straight structures with geometric nonlinearities *J. Fluids and*  
545 *Structures*, 26, 1098-1122.
- 546 Williamson, C. H. K. **1996** Vortex dynamics in the cylinder wake *Annu.*  
547 *Rev. Fluid Mech.*, 28, 477-539.